Resonance Raman Studies of Cytochrome P450 2B4 in Its Interactions with Substrates and Redox Partners[†]

Piotr J. Mak,[‡] Sang-Choul Im,[§] Haoming Zhang,[§] Lucy A. Waskell,*[,§] and James R. Kincaid*[,‡]

Chemistry Department, Marquette University, Milwaukee, Wisconsin 53233, and Department of Anesthesiology, University of Michigan and VA Medical Center, Ann Arbor, Michigan 48105

Received January 7, 2008; Revised Manuscript Received January 30, 2008

ABSTRACT: Resonance Raman studies of P450 2B4 are reported for the substrate-free form and when bound to the substrates, benzphetamine (BZ) or butylated hydroxytoluene (BHT), the latter representing a substrate capable of inducing an especially effective conversion to the high-spin state. In addition to studies of the ferric resting state, spectra are acquired for the ferrous CO ligated form. Importantly, for the first time, the RR technique is effectively applied to interrogate the changes in active site structure induced by binding of cytochrome P450 reductase (CPR) and Mn(III) cytochrome b_5 (Mn cyt b_5); the manganese derivative of cyt b_5 was employed to avoid spectroscopic interferences. The results, consistent with early work on mammalian P450s, demonstrate that substrate structure has minimal effects on heme structure or the FeCO fragment of the ferrous CO derivatives. Similarly, the data indicate that the protein is flexible and that substrate binding does not exert significant strain on the heme peripheral groups, in contrast to $P450_{cam}$, where substantial effects on heme peripheral groups are seen. However, significant differences are observed in the RR spectra of P450 2B4 when bound with the different redox partners, indicating that the heme structure is clearly sensitive to perturbations near the proximal heme binding site. The most substantial changes are displacements of the peripheral vinyl groups toward planarity with the heme macrocycle by cyt b_5 but away from planarity by CPR. These changes can have an impact on heme reduction potential. Most interestingly, these RR results support an earlier observation that the combination of benzphetamine and cyt b_5 binding produce a synergy leading to unique active site structural changes when both are bound.

Mammalian cytochromes P450 (P450)[1] are involved in many critical physiological processes, including oxidative transformation of drugs, pollutants, and other exogenous and endogenous chemicals (*1–3*). The P450 2B family of enzymes, in general, and particularly P450 2B4, has attracted much attention as a model system for the elucidation of essential structure–function relationships (*4, 5*). The active site of all P450s contains a cysteine−thiolate-ligated ferric protoheme, whose principally low-spin resting state is transformed with varying efficiencies into a high-spin configuration upon binding of different substrates. This redox-poised high-spin state is reduced by associated redox partners to generate a ferrous species that rapidly forms a rather unstable dioxygen adduct. Following transfer of a second electron, a meta-stable ferric peroxo fragment is produced. Upon further protonation and heterolytic cleavage of the oxygen bond, a highly oxidizing ferryl heme π-cation radical, usually referred to as Compound I, is formed (*2, 3, 6, 7*). In the case of P450 2B4, the ferric protein is reduced by cyt P450 reductase while the oxyferrous protein can be reduced by either cyt b_5 or the reductase.

One primary issue of interest in studying the P450 enzymatic mechanism is the extent to which heme structure and reactivity are influenced by substrate structure, and of the techniques applicable to this question, resonance Raman (RR) spectroscopy has proven itself to be an especially useful probe of the active site, permitting documentation of oxidation and spin-state distributions and macrocycle structure, as well as reporting on the disposition of the key linkages between the central iron and the axial thiolate ligand or various diatomic exogenous ligands, including CO, NO, and, in certain cases, the $Fe-O_2$ fragment (*8–11*). While this powerful spectroscopic technique was effectively applied in many studies of bacterial P450s early on (*12–20*), problems with sample purification and enzyme solubility hampered and delayed comparable studies of the mammalian proteins (*21–26*). Fortunately, the development of effective procedures for the expression and purification of certain mammalian P450s has resulted in a renewed interest in RR studies of these physiologically important systems (*27–31*).

[†] This work was supported in part by National Institutes of Health Grants DK35153 (to J.R.K.) and GM35533 (to L.A.W.) and by a VA Merit Review Grant (to L.A.W.).

* To whom correspondence should be addressed. J.R.K.: tel, (414) 288-3539; fax, (414) 288-7066; e-mail, james.kincaid@marquette.edu. L.A.W.: tel, (734) 845-5858; fax, (734) 845-3096; e-mail, waskell@med.umich.edu.

[‡] Marquette University.

[§] University of Michigan and VA Medical Center.

[1] Abbreviations: P450, cytochrome P450; BZ, benzphetamine; BHT, butylated hydroxytoluene; cyt b_5, cytochrome b_5; Mn cyt b_5, cytochrome b_5 reconstituted with Mn protoporphyrin IX; DLPC, dilauroyl-L-α-phosphatidylcholine; DTT, dithiothreitol; CPR, cytochrome P450 reductase; RS, resting state of ferric protein; RR, resonance Raman; oop, out of plane; 5CHS, five-coordinated high spin; 6CLS, six-coordinated low spin; Mb, myoglobin; SF, substrate-free; MLCT, metal-to-ligand charge transfer; LMCT, ligand-to-metal charge transfer.

10.1021/bi800034b CCC: $40.75
Published on Web 03/01/2008

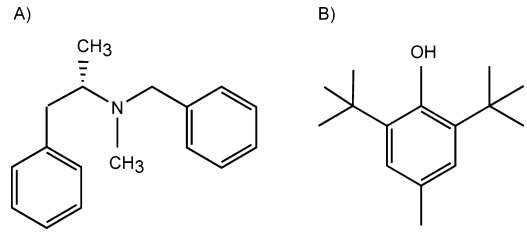

FIGURE 1: Chemical structures of substrates: (A) benzphetamine (BZ) and (B) butylated hydroxytoluene (BHT).

An intriguing finding that emerged in the study of the paradigmatic P450 2B4 is the observation that cytochrome b_5 (cyt b_5) and P450 reductase affect cyt P450 catalyzed reactions in different ways (*1, 5*). Though cyt b_5 and cytochrome P450 reductase (CPR) reduce the oxyferrous P450 2B4 at the same rate, substrate oxidation proceeds more slowly for the P450 2B4−CPR complex (*5*). Thus, it is of great interest now to attempt to interrogate and compare the active site heme structures of P450 2B4 complexed with either cyt b_5 or CPR for the resting, ferric state and various intermediates in the enzymatic cycle.

The present work reports detailed RR studies of the heme structure for P450 2B4 in the substrate-free form and bound to either of two different substrates, benzphetamine (BZ) or butylated hydroxytoluene (BHT) (Figure 1), the latter representing a substrate capable of inducing an especially effective conversion to the high-spin state (*32*). In addition, for the first time, the RR technique is effectively applied to interrogate the changes in active site structure that are induced by binding the two different redox partners, i.e., CPR and Mn(III) cytochrome b_5 (Mn cyt b_5), the manganese derivative being employed to avoid complications involving interference by RR lines of the native (iron-containing) cyt b_5 (*33*). The results demonstrate that substrate structure has minimal effects on heme structure and only small effects on the ν(Fe−C) frequency of the FeCO fragment, results consistent with early work on mammalian (*30, 31, 34*) and related systems (*35*). However, significant differences are seen here in the RR spectra of both the ferric and ferrous CO forms of P450 2B4 when bound with the different redox partners, indicating that the heme structure and inherent reactivity are clearly sensitive to perturbations near the proximal heme binding site. Of special interest is the fact that the RR data obtained here provide the first spectroscopic evidence for a unique active site structure associated with the simultaneous binding of BZ and cyt b_5, this combination having previously been shown to exhibit synergistic functional behavior (*5*). Thus, binding of Mn cyt b_5 to the BZ-bound 2B4 leads to changes in low-frequency vinyl bending modes that reflect higher population of in-plane orientations of vinyl groups with respect to the heme macrocycle, changes that can have functional consequences.

MATERIALS AND METHODS

(A) Protein Preparation. (1) Expression and Purification. (a) Materials. Aprotinin, benzphetamine, dithiothreitol (DTT), EDTA, sodium dithionite, 2,4-di-*tert*-butyl-4-methylphenol (butylated hydroxytoluene, BHT), DEAE-resin, and octyl-Sepharose resin were purchased from Sigma-Aldrich. Bio-Beads and hydroxyapatite resins were purchased from Bio-Rad. C41 *Escherichia coli* cells were from Avidis (Saint Beauzire, France) (*36*). Dilauroyl-L-α-phosphatidylcholine (DLPC) was purchased from Doosan Serdary Research Laboratories (Toronto, Canada). Glycerol and the protease inhibitor cocktail tablets were purchased from Roche Diagnostics. The Roche Diagnostics glycerol was purified further, first by treating it with activated charcoal and then by distilling it. All other chemicals were purchased from Fisher (Fair Lawn, NJ).

(b) Protein Expression and Purification. Plasmids, pLW01-b5mem and pLW01-P450 2B4 mem, were used for expression of wild-type full-length rabbit cyt b_5 and wild-type full-length rabbit P450 2B4, respectively (*37*). Both plasmids contained the β-lactamase, ampicillin resistance gene, and the cyt b_5 and P450 2B4 genes were downstream of a T7 promoter. Plasmid pSC263-ratCPR with the eight extra amino acids (GIPGDPTN) deleted from the N-terminus of Dr. Shen's pOR263-rat CPR plasmid was used for the expression of wild-type full-length rat NADPH cytochrome P450 reductase (CPR) (*38*). Cyt P450 2B4 and cyt b_5 were expressed in C41 *E. coli* cells and purified as previously described (*36, 37, 39*). Manganese cyt b_5 (Mn cyt b_5) was prepared from the full-length *apo* rabbit cyt b_5 by reconstituting it with Mn protoporphyrin IX as previously described (*40*). The CPR was also expressed in C41 *E. coli* cells and purified without using a 2′,5′-ADP affinity column by a modification of the procedure of Kasper and colleagues (*38*). Briefly, harvested cells were resuspended in buffer A (50 mM Tris−acetate, pH 7.7 at 25 °C, 0.2 mM DTT, 0.1 mM EDTA, 1 μg/mL aprotinin or protease inhibitor cocktail tablet, 1 μM FMN, and 10% glycerol) and were lysed by sonication in an ice/salt bath. The purification was performed at 4 °C. The membrane fraction was obtained by centrifugation of the cell lysate at 100000*g* for 1 h at 4 °C. The membrane-containing pellet was resuspended with buffer A and solubilized by stirring with 0.3% Triton X-100 (v/v) for ≅3 h at 4 °C. The solubilized proteins were obtained from the supernatant after another centrifugation at 100000*g* for 1 h at 4 °C. The solubilized membrane solution was loaded directly onto a DEAE column which was then washed with buffer B [50 mM Tris−acetate, pH 7.7 at 25 °C, 0.1% Triton X-100 (v/v), 0.2 mM DTT, 0.1 mM EDTA, 1 μM FMN, 0.17 M NaCl, and 10% glycerol] until all of the contaminating cytochrome (detected at 420 nm) had eluted. The reductase was then eluted with a salt gradient from 0.17 to 0.5 M NaCl in buffer B. All of the fractions lacking cytochromes (detected at 420 nm) were loaded onto a Bio-Beads column followed by an octyl-Sepharose column. The two columns, which were connected to each other, had been preequilibrated with buffer B containing 0.1% sodium cholate instead of Triton X-100. The octyl-Sepharose column was washed with the loading buffer until the contaminating orange color of an unknown protein had eluted.

The CPR was eluted from the octyl-Sepharose column with buffer C [potassium phosphate, pH 7.4, 0.3% Triton X-100 (v/v), 0.2 mM DTT, 0.1 mM EDTA, 1 μM FMN, and 20% glycerol]. The CPR-containing eluate was diluted 3-fold with cold water containing 1 μM FMN and 20% glycerol. Potassium ferricyanide (≅50% molar excess with respect to CPR) was added to oxidize the reductase. The oxidized reductase was loaded onto a hydroxyapatite column previously equilibrated with 5 mM potassium phosphate buffer, pH 7.4, containing 1 μM FMN and 20% glycerol.

The column was washed with the loading buffer to remove the detergent until the OD at 280 nm was less than 0.005. The bright yellow reductase was eluted with 400 mM potassium phosphate buffer, pH 7.4, containing 20% glycerol. The purified reductase had a specific content of 12.8 nmol of P450 reductase/mg of total protein and a single band on a SDS−polyacrylamide gel.

The concentration of P450 2B4 was determined using an extinction coefficient $\Delta\epsilon_{450-490nm}$ of 91 mM^{-1} cm^{-1} for the P450 2B4−CO complex, as described by Omura and Sato (*41*). Only samples of P450 2B4 having an A_{420}/A_{280} ratio greater than 1.84 were used for the resonance Raman experiments. The concentration of CPR was determined using an extinction coefficient of 21.4 mM^{-1} cm^{-1} at 456 nm for fully oxidized protein (*42*). The concentration of cyt b_5 was determined using an extinction coefficient of 185 mM^{-1} cm^{-1} for the absorbance change at 426 nm minus 409 nm between ferrous and ferric cyt b_5, respectively (*43*). The concentration of Mn^{3+} cyt b_5 was calculated using an extinction coefficient of 57 mM^{-1} cm^{-1} at 468 nm (*33, 40*).

(2) Preparation of Raman Samples. The purified proteins (P450, Mn cyt b_5, CPR) were concentrated using a Vivaspin concentrator (Viva Science) with a 10000 molecular weight cutoff in a swinging bucket rotor in a Sorvall centrifuge at 3000*g* at 4 °C. The proteins were resuspended in the buffer used for Raman measurements (100 mM potassium phosphate, pH 7.4, 1 mM DLPC, 20% purified glycerol). This process was repeated five times to concentrate the proteins (all proteins present at ≅1.2 mM). These concentrated, oxidized proteins at ≅1.2 mM were diluted with the Raman buffer to a final concentration of 150 μM (i.e., for samples having multiple proteins, the concentration of each protein is 150 μM). It is pointed out that, at the concentrations of the full-length P450 2B4 being used here, the P450 does not dimerize with the imidazole of His 226 bound to the heme iron of the second molecule of P450 2B4 as it does at the high concentrations used during crystallization (*44*). Furthermore, the K_d values between P450 2B4 and cyt b_5 and CPR are 0.2 μM and 0.02 μM, respectively (*5, 37*). Therefore, at the higher concentrations employed here, it is expected that close to 100% of the P450 2B4 is bound with reductase. When present, the final concentration of the substrate, benzphetamine or butylated hydroxytoluene, was 900 μM. The butylated hydroxytoluene was added from a 0.6 M solution in 50% aqueous methanol to give a final methanol concentration of ≅0.075% in the butylated hydroxytoluene-bound samples used for Raman spectroscopy.

Carbonmonoxy complexes of ferrous P450 were prepared without and with the substrates, benzphetamine and butylated hydroxytoluene. The final protein concentration was 150 μM whereas the final substrate concentration was 900 μM. When present, Mn^{3+} cyt b_5 and CPR were added at an equal molar ratio to cyt P450. To prepare the carbonmonoxy ferrous P450 2B4 samples, a deoxygenated sample containing ferric P450 and the appropriate substrate and protein additives were reduced in a glovebox with a standardized solution of sodium dithionite. The P450 samples were reduced with a stoichiometric amount of a standardized solution of sodium dithionite. The cyt P450−Mn cyt b_5 complex was also reduced with a stoichiometric amount of a standardized solution of sodium dithionite. The P450−CPR complex was reduced with three electron equivalents from sodium dithionite (to generate ferrous P450 and two-electron-reduced reductase). An approximately 50% molar electron equivalent excess with respect to P450 was added to all reduced samples to prevent oxidation by trace amounts of oxygen. The reduced P450 solution with the desired additives was transferred within the glovebox to a 5 mm NMR tube (WG-5 Economy; Wilmad), which was sealed with a natural rubber septum from Sigma-Aldrich. The reduced samples in the NMR tubes were removed from the glovebox, and CO gas was bubbled slowly through the solution for ≅30 s. The samples were immediately frozen and stored in liquid nitrogen until being shipped to Marquette University at −196 °C in a "dry shipper" (Taylor-Wharton Cryogenics, CX-100) where they were examined by Raman spectroscopy.

(B) Resonance Raman Measurements. The RR spectra of all samples were measured using a Spex 1269 spectrometer equipped with an Andor Newton EMCCD detector (Model DU971; Andor Technologies). The 406.7 nm line from a Kr^+ laser (Coherent Innova Model 100-K3) was used for excitation of ferric P450 2B4 samples. The 441.6 nm excitation line that was used for probing P450 Fe(II)−CO adducts was provided by a He−Cd laser (Liconix Model 4240), while the 363.8 nm line from an Ar^+ laser (Spectra Physics, Model 2025-05) was used as the excitation source in order to observe the Fe−S stretch (*14*). The laser power at the sample was maintained at around 1 mW for the CO adducts, while the power used for ferric samples was adjusted to ∼8 mW. The samples were contained in spinning NMR tubes (WG-5, Economy; Wilmad) in order to avoid the laser-induced protein degradation and photodissociation of CO from the ferrous CO samples. Spectra were calibrated with fenchone and processed with Grams/*32* AI software. Measurements were done using 180° backscattering, and the laser beam was focused on the sample using a cylindrical lens. The sample-containing NMR tube was placed in a homemade quartz dewar filled with water at different temperatures (4 and 30 °C). The temperature was monitored using a thermocouple and did not change during the measurements by more than ±2 °C.

RESULTS AND DISCUSSION

(A) Ferric P450 2B4 and Its Interactions with Substrates and Redox Partners. (1) Effects of Substrate on Ferric P450 2B4. (a) High-Frequency Resonance Raman Spectra. The high-frequency resonance Raman (RR) spectra of substrate-free (spectra A and B) and substrate-bound [benzphetamine (BZ), spectra C and D, and butylated hydroxytoluene (BHT), spectra E and F] at 4 and 30 °C are presented in Figure 2. The RR spectra were normalized to the glycerol band observed at 1467 cm^{-1}. The RR modes in the high-frequency region were assigned to vibrations of certain molecular fragments employing previously reported assignments of vibrational modes of substrate-free P450 2B4 as well as assignment of vibrational modes of Ni-octaethylporphyrin (*23, 45, 46*).

This region of the resonance Raman spectra includes oxidation state and spin-state markers. In the spectra of the substrate-free form at 4 °C the 1372 cm^{-1} ν_4 frequency indicates the ferric state, while the ν_3 modes observed at 1487 cm^{-1} and 1502 cm^{-1} show that the substrate-free P450 2B4 at 4 °C exists in equilibrium between five-coordinated high-

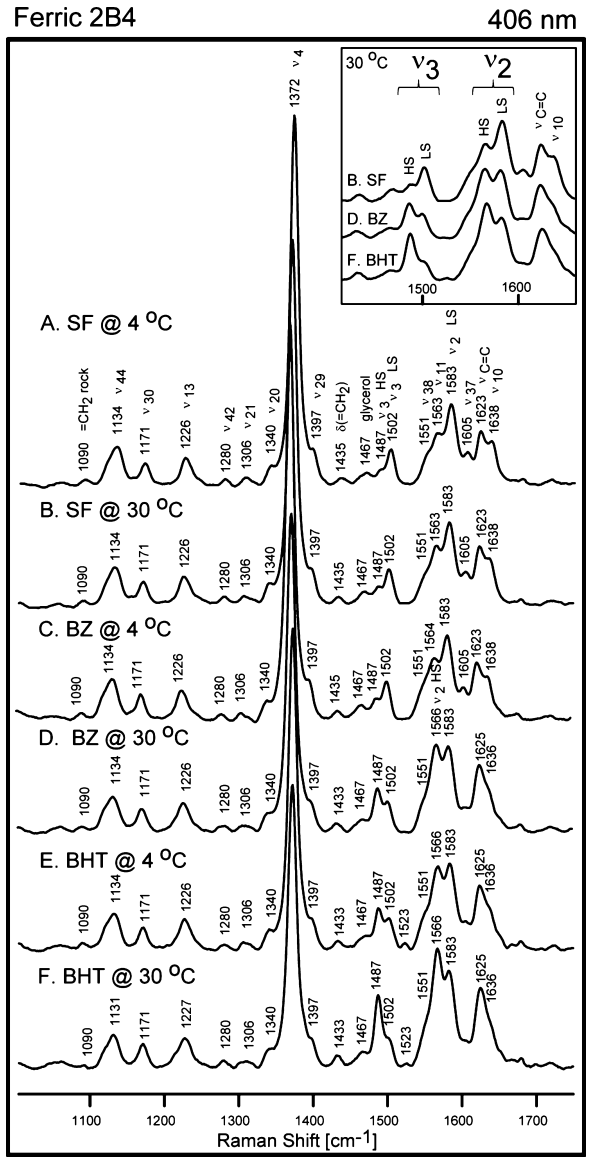

FIGURE 2: High-frequency resonance Raman spectra of wild-type resting state (RS) ferric P450 2B4 without [substrate-free (SF)] (spectra A and B) and with substrates [spectra C and D with benzphetamine (BZ); spectra E and F with butylated hydroxytoluene (BHT)] at 4 and 30 °C. Excitation line 406 nm, 8 mW on the sample, total collection time 10 min (spectra normalized to glycerol band at 1467 cm^{-1} mode). The inset shows an expanded region of spin-state markers.

spin (5CHS) and six-coordinated low-spin (6CLS) forms, respectively (Figure 2A). The relative intensity of the 1487 cm^{-1} band is smaller compared to the more dominant 1502 cm^{-1} mode. The additional spin-state markers in this region, ν_2 and ν_{10}, are observed at 1583 and 1638 cm^{-1}, respectively. Increasing the temperature to 30 °C does not lead to substantial changes in the percentage of low- and high-spin components for substrate-free P450 2B4 (Figure 2B).

BZ and BHT are both good substrates for P450 2B4. BZ has a k_{cat} of ~50 with ~50% coupling of NADPH consumption to product formation (*5, 47*), while BHT has a k_{cat} of ~36 with a coupling of ~30% (Waskell et al., unpublished data). Thus, it is not surprising that addition of BZ or BHT increases the high-spin component at 4 °C (Figure 2C,E), as judged by the noticeable increase in intensity of the ν_3 mode at 1487 cm^{-1} (especially in the case of BHT), compared to that observed in the spectra of the substrate-free sample at 4 °C. The increase in temperature in both of the substrate-bound samples to 30 °C results in even higher conversion to high-spin form, although the low-spin fraction (1502 cm^{-1}) is still present in both spectra (Figure 2D,F). The increase in high-spin form at the higher temperatures is attributed to enhanced binding of the substrates since hydrophobic forces, which are important for substrate binding, are greater and the tertiary amine of BZ is less protonated at the elevated temperature. The increase in the ν_3 high-spin component is accompanied by the appearance of a new band at 1566 cm^{-1}, characteristic of a high-spin ν_2 mode and is most clearly observed in the spectra of BZ at 30 °C and for BHT-bound at 4 and 30 °C. This mode actually overlaps with the depolarized (B_{1g}) ν_{11} mode normally observed near 1560 cm^{-1}, which contains substantial contributions from $\nu(C_\beta-C_\beta)$ and is slightly sensitive to spin-state changes, the overlap of the two modes resulting in an apparent shift to slightly higher frequency as the percentage of high-spin component increases; i.e., compare traces D−F with traces A−C in Figure 2.

The region between ~1620 and 1640 cm^{-1} consists of an envelope of four components. A low-spin ν_{10} is expected near 1640 cm^{-1}, with the high-spin ν_{10} being expected near 1625 cm^{-1} (*8, 9*). In addition, for P450 2B4, two vinyl modes have been previously observed with frequencies at 1622 and 1629 cm^{-1} (*25, 26*). Thus, as the spin-state equilibrium changes in proceeding down the series of traces, the changing envelope reflects the fact that the intensity of the low-spin component near 1638 cm^{-1} diminishes as the intensity of the high-spin component, presumed to occur near 1625 cm^{-1}, shows a corresponding increase, noting again that this high-spin ν_{10} mode overlaps with the two vinyl modes in this region. While some early works reported changes in intensities of the two vinyl modes upon substrate binding (*24, 26*), work performed with higher resolution conditions did not confirm such effects, showing no such intensity changes upon substrate binding (*25*), a result consistent with the data presented here. The frequencies of all of the heme modes in the region between 1000 and 1350 cm^{-1}, as well as the bands assigned to ν_{29} at 1397 cm^{-1} and ν_{38} at 1551 cm^{-1}, none of which are effective spin-state marker modes, maintain constant frequencies in all of the observed spectra.

(b) Low-Frequency Resonance Raman Spectra. In the low-frequency region of the RR spectra, modes associated with coordinated axial ligands can be enhanced by resonance with various MLCT or LMCT transitions or by excitation within the strong Soret $\pi-\pi^*$ transition (*8*) permitting RR monitoring of the key linkages between the heme prosthetic group and exogenous ligands or the endogenous ligands provided by the associated protein, such as the $Fe-S_{cysteine}$ linkage of interest here (*9, 14*). Additionally, in recent years, it has become increasingly apparent that certain low-frequency heme modes, including bending motions of the vinyl or propionate substituents and out-of-plane modes (γ_i) activated by distortions of the heme macrocycle from planarity, are especially sensitive to changes in active site structure brought about by binding of substrates, effectors, or other proteins; i.e., these modes provide direct evidence of active site perturbations (*35, 45, 48, 49*).

The low-frequency RR spectra of P450 2B4 in the resting state and substrate-free and substrate-bound forms at 4 and 30 °C are shown in Figure 3. On the basis of the fact that

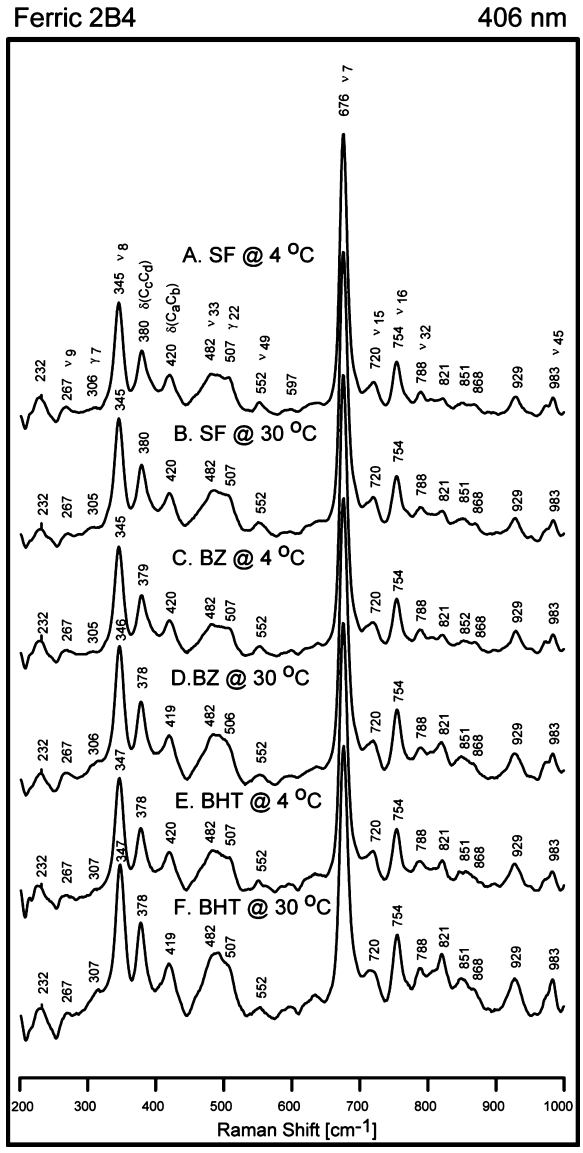

FIGURE 3: Low-frequency resonance Raman spectra of wild-type ferric P450 2B4 without (spectra A and B) and with substrates [spectra C and D with benzphetamine (BZ); spectra E and F with butylated hydroxytoluene (BHT)] at 4 and 30 °C. Excitation line 406 nm, 8 mW on the sample, total collection time 15 min (spectra normalized to the ν_7 mode).

the high-frequency RR bands of both the high-spin and low-spin forms are significantly enhanced with the 406 nm excitation line being used here, it is reasonable to assume that the low-frequency spectra may contain contributions from both forms. Nevertheless, inspection of the spectral data displayed in Figure 3 makes it quite clear that addition of substrates to the P450 2B4 protein does not lead to many significant changes in the low-frequency modes, the most noticeable being the apparent, but very slight, intensity increases in the γ_7 mode near 305 cm^{-1} and perhaps within the envelope of bands between 482 and 507 cm^{-1}.[2] Although such weak features have been observed in the 470–510 cm^{-1} region in the RR spectra of several other cytochromes P450 (*16, 23, 28–30*), they were not discussed and no assignments were made. However, the assignments of modes near 500 cm^{-1} have been made for several other heme proteins. Thus, Hu et al. (*48*) assigned a 499 cm^{-1} feature to γ_{22} in the RR spectrum of deoxymyoglobin, noting it shifts to 502 cm^{-1} in the spectrum of metMb. In a later work (*49*), involving myoglobins reconstituted with protohemes bearing deuterated methyl groups, this assignment was confirmed, and a mode appearing near 490 cm^{-1} for deoxy-Mb was assigned to ν_{33}, which had been previously observed at 475 cm^{-1} for met-Mb (*48*). These assignments and those for other vibrational modes in this region are all based on previous assignments made for isotopically labeled heme proteins and model compounds (*45, 46, 48–50*), as well as those made for substrate-free P450 2B4 (*23*). The only other changes that occur upon binding of benzphetamine or butylated hydroxytoluene are the quite small (1–2 cm^{-1}) upshift of the ν_8 mode and small downshifts (1–2 cm^{-1}) of propionate and vinyl modes (Figure 3D−F).

The lack of any substantial changes in the low-frequency RR spectra upon substrate binding to the mammalian P450 2B4 protein is in contrast to the behavior seen for bacterial P450s, where rather substantial changes in frequencies and intensities, as well as the appearance of new modes, are often observed upon substrate binding; the new modes are normally ascribed to propionate mode shifts (from about 380 cm^{-1} to 366 cm^{-1}) associated with H-bonding changes (*18*) and to activation of out-of-plane (oop) modes associated with heme deformation (*35, 45*). On the other hand, the lack of substantial shifts documented here is consistent with previous RR studies of other mammalian P450s. Thus, in a study of P450 2B4 (formerly referred to as P450LM2) by Hildebrandt and co-workers, no significant (>1 cm^{-1}) changes were observed between low-frequency RR spectra of substrate-free and benzphetamine-bound samples (*25*). A similar lack of changes upon addition of substrates was noted in the case of human cytochrome P450 2D6 and its F120A mutant (*29*). However, this lack of low-frequency response upon substrate binding is not uniformly characteristic for all mammalian P450s; e.g., some significant changes (by as much as 6 cm^{-1}) upon substrate binding have been reported for human P450 aromatase and mitochondrial P450scc, specifically for modes involving the propionate and vinyl substituents (*25, 28*). In the case of P450 2B4, the relatively open and flexible heme pocket required for accommodating large and structurally diverse substrates obviously may not be likely to exert significant substrate-induced strain on heme peripheral groups.

Another important structural element of interest is the linkage between the heme iron and the cysteine thiolate ligand, which can be interrogated with near-UV excitation (*14*). The three upper traces presented in Figure 4 show low-frequency RR spectra, excited with the 363.8 nm laser line, of ferric P450 2B4 samples with BHT or BZ bound, as well as substrate-free. The spectra with BZ or BHT bound show a strong band at 354 cm^{-1} that is assignable to the ν(Fe−S) mode (spectra A and B) (*14, 51*), while the spectrum of substrate-free exhibits only a weak feature in this region that is reasonably attributed to the heme ν_8 mode, based on the similarity of its frequency to the ν_8 mode seen in the RR spectra of ferric samples with visible excitation (Figure 3). This relatively weak sensitivity of the ν(Fe−S) mode to

[2] While an internal mode of the glycerol solution component is known to occur at ~485 cm^{-1}, it is expected to make an insignificant contribution to these spectra, given its inherently weak intensity relative to other glycerol bands at ~821 and 850 cm^{-1}, which are seen as fairly weak features in the spectra acquired here.

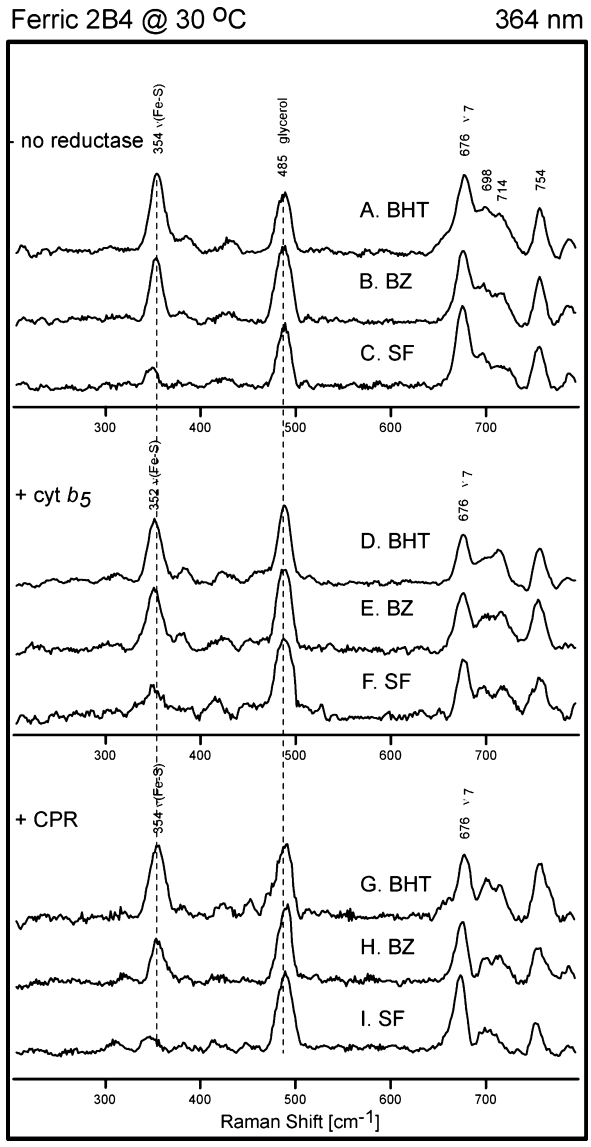

FIGURE 4: The low-frequency RR spectra of ferric BHT and BZ bound as well as substrate-free 2B4 without redox partner (A−C), with Mn cyt b_5 (D−F), and with P450 reductase (G−I) present. Excitation line 364 nm, total collection time for each spectra 30 min.

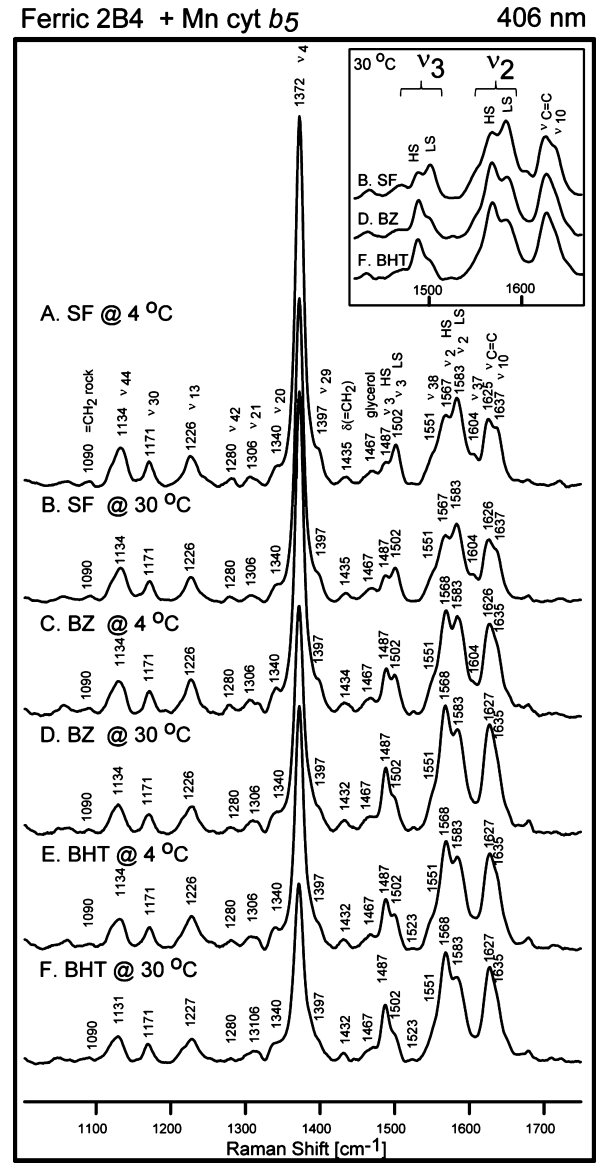

FIGURE 5: High-frequency resonance Raman spectra of wild-type cyt P450 2B4 without (spectra A and B) and with substrates [spectra C and D with benzphetamine(BZ); spectra E and F with butylated hydroxytoluene (BHT)] at 4 and 30 °C in the presence of Mn(III) cyt b_5. Excitation line 406 nm, 8 mW on the sample, total collection time 10 min (spectra normalized to glycerol band at 1467 cm^{-1} mode). The inset shows an expanded region of spin-state markers.

substrate structure is not surprising, given the results observed for other P450 enzymes. Thus, the frequency of the Fe−S stretch in P450cam was affected only by ≤1 cm^{-1} upon addition of camphor, adamantanone, norcamphor or TMCH (3,3,5,5-tetramethylcyclohexanone) (*51*). On the other hand, there has been one report of more significant effects in the case of the mammalian protein, human P450 aromatase, where the ν(Fe−S) was found to vary from 344 to 349 cm^{-1} in the presence of various substrates (*28*). The important point to be made is that in the case of P450 2B4 and the bacterial protein mentioned above, structural variations in the substrate, which resides in the distal pocket, have little effect on the status of the Fe−S fragment.

(2) Effect of Redox Partners: Mn(III) Cyt b_5 and Cytochrome P450 Reductase on Ferric P450 2B4. (a) High-Frequency Resonance Raman Spectra. Figures 5 and 6 show the high-frequency resonance Raman spectra of substrate-free and substrate-bound forms of P450 2B4 interacting with Mn(III) cytochrome b_5 (Mn cyt b_5) and rat P450 reductase, respectively. The spectra are normalized to the glycerol mode observed at 1467 cm^{-1}. As can be seen by comparing corresponding traces in Figures 2 and 5, the presence of Mn cyt b_5 has definite, though variable, effects on the spin-state equilibria, generally leading to increases in the percentage of high-spin component, even slightly increasing the high-spin markers for the substrate-free form at 30 °C (compare trace B in each figure). While the ν_3 and ν_2 intensities are also only slightly greater for the BHT-bound forms (traces E and F of Figures 2 and 5), substantially greater effects of the Mn cyt b_5 are seen for the BZ-bound form, as evidenced by the obvious increases in intensities of the 1487 and 1568 cm^{-1} features in traces C and D of Figure 5, compared to their intensities in Figure 2, the increases being especially great for the data acquired at 4 °C, as seen in trace C of each figure. Thus, the present results provide evidence for a

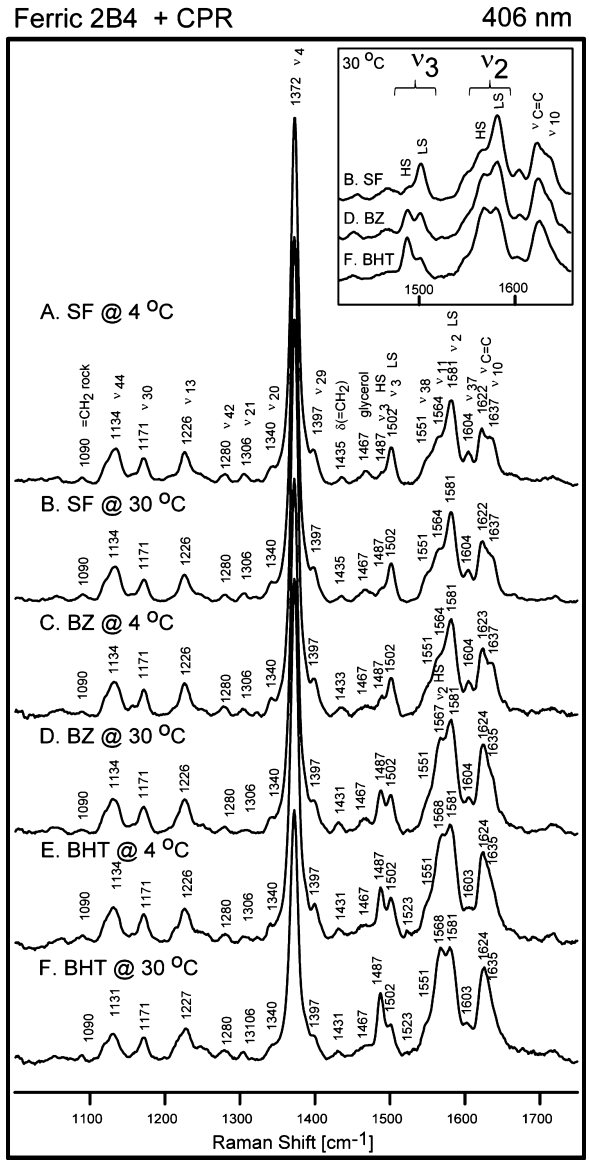

FIGURE 6: High-frequency resonance Raman spectra of wild-type cyt P450 2B4 without (spectra A and B) and with substrates [spectra C and D with benzphetamine (BZ); spectra E and F with butylated hydroxytoluene (BHT)] at 4 and 30 °C in the presence of P450 reductase. Excitation line 406 nm, 8 mW on the sample, total collection time 10 min (spectra normalized to glycerol band at 1467 cm^{-1} mode). The inset shows an expanded region of spin-state markers.

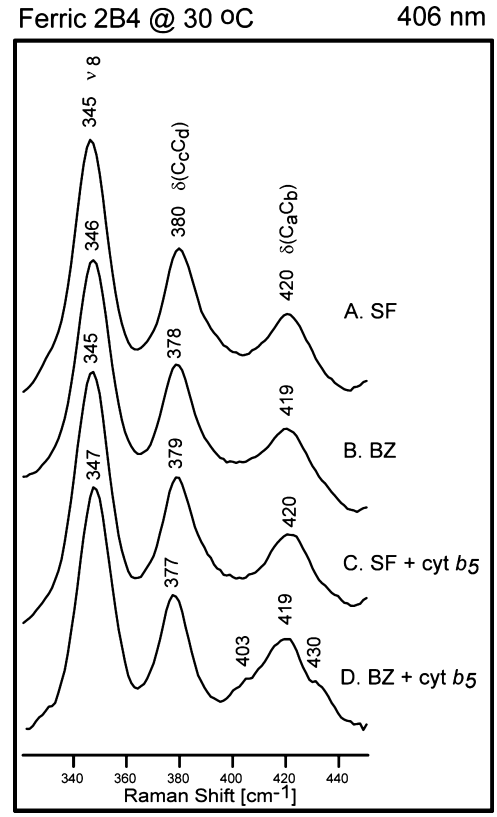

FIGURE 7: Expanded (320–450 cm^{-1}) region of low-frequency resonance Raman spectra of ferric P450 2B4 substrate-free, BZ-bound, substrate-free with Mn cyt b_5 present, and BZ-bound with Mn cyt b_5 present (the two upper spectra are taken from Figure 3 and the two bottom spectra are taken from Figure S1). Excitation line 406 nm, 8 mW on the sample, total collection time 15 min.

synergistic effect of cyt b_5 and BZ; i.e., the BZ effect documented in traces C and D in Figure 2 is enhanced by the presence of Mn cyt b_5, as shown in the corresponding traces in Figure 5. Such effects are consistent with previous work that suggested such synergistic interactions for simultaneous binding of BZ and cyt b_5 (*5, 52, 53*). The Mn cyt b_5 interaction with the P450 2B4 protein also gives rise to changes in the 1620–1640 cm^{-1} region, containing the contributions from ν(C═C) of the vinyl groups and the ν_{10} mode, as expected based on the discussion given above regarding the 10–12 cm^{-1} downshift of ν_{10}.

Interestingly, the P450 reductase does not substantially enhance the percentage of high-spin component and in fact seems to cause a small decrease in the high-spin component, comparing Figures 2 and 6, with the apparent changes in the ratio of the ~1568 and 1581 cm^{-1}, ν_2, modes being most obvious and then only for the samples having a substantial high-spin component, i.e., traces D−F.

(b) Low-Frequency Resonance Raman Spectra. The low-frequency RR spectra of substrate-free and substrate-bound P450 2B4 interacting with Mn cyt b_5 and CPR are shown in Supporting Information Figures S1 and S2, respectively. There it is seen that the addition of Mn cyt b_5 appears to increase the intensity of γ_7 for the BZ- and BHT-bound samples (traces C−F in Figure S1) relative to those seen in Figure 3, but the effect is really quite small, implying insubstantial out-of-plane distortions of the heme macrocycle. One clearly noticeable effect however, as seen in Figure 7, occurs when both BZ and the Mn cyt b_5 are present, where two new vinyl bending modes are activated, noting that the effect is enhanced for the 30 °C samples relative to that at 4 °C, confirming its validity, the enhancement being associated with more effective substrate binding at 30 °C, as was observed above for samples without reductase present. Again, these RR spectra reveal active site structural changes that occur only for this BZ/cyt b_5 combination.

Regarding any potential impact of reductase binding on the key Fe−S_{Cys} linkage, the addition of Mn cyt b_5 (traces D−F in Figure 4) does cause a slight (2 cm^{-1}) shift to lower frequency for the ν(Fe−S) modes in both samples of substrate-bound, compared to the 354 cm^{-1} value in traces A and B, while addition of CPR (traces G−I) does not change the position of the Fe−S stretch. In the only other study comparable to the present investigation of redox partner interactions, P450cam in the presence of its natural redox

partner, putidaredoxin, exhibited a shift of ~3 cm^{-1} to *higher* frequency for ν(Fe−S), a shift that occurred in concert with an increase in low-spin component (*51*). This observation is consistent with data reported here for Mn cyt b_5, which decreases the low-spin component while simultaneously lowering the ν(Fe−S). Consistent with this is the fact that binding of CPR has only a relatively small effect on the spin-state distribution and no significant effect on ν(Fe−S). Thus, whatever structural features give rise to an increased high-spin population also lead to a decreased Fe−S bond strength and vice versa.

In the earlier study of putidaredoxin (Pd) binding to P450cam (*51*), the increase in ν(Fe−S) was attributed to decreased net positive charge on the proximal surface of the enzyme that resulted from binding of the negatively charged surface of the Pd; i.e., the reduced positive charge is considered to enhance the negative charge density on the sulfur donor group, strengthening the Fe−S linkage. Inasmuch as similar charge balance considerations are applicable to the proteins of interest here, the 2B4 having positive proximal charges and both reductases negatively charged interacting surfaces (*5, 52, 54*), the arguments based on electrostatics cannot explain the *decreased* frequency observed for the ν(Fe−S) upon binding of Mn cyt b_5. Thus, the fact that both redox partners present negatively charged surfaces to the proximal surface of P450 2B4, with one inducing no shift and the other causing a shift in the opposite direction to that expected on the basis of electrostatic arguments, leads to the conclusion that the Mn cyt b_5 protein induces specific structural changes at the 2B4 proximal surface that propagate to the heme group leading to a weakened Fe−S linkage.

(B) Ferrous CO P450 2B4 Adduct and Its Interaction with Substrates and Redox Partners. (1) Effect of Substrate on Ferrous CO P450 2B4. The low-frequency RR spectra of the ferrous CO adducts of substrate-free and both substrate-bound forms of P450 2B4 at 4 and 30 °C are shown in Figure 8. The spectra are normalized to the ν_7 mode at 673 cm^{-1} and were acquired with a 442 nm excitation line, in close resonance with the 446 nm Soret absorption band. The most dominant band in this region, besides the ν_7 mode, is the ν(Fe−CO) stretch that is found at 472 cm^{-1} in the spectrum of the substrate-free sample at 4 °C. The band at 558 cm^{-1} is assigned to the δ(Fe−C−O) bending mode (Figure 8A). As the temperature is raised, those two modes shift down only by ~1 cm^{-1}. The addition of benzphetamine to the sample induces a 2 cm^{-1} downshift of ν(Fe−CO) relative to the substrate-free sample, while on the other hand, the addition of butylated hydroxytoluene causes a slight (2 cm^{-1}) shift of this mode to *higher* frequency, a shift in this direction normally being taken to imply some increase in distal pocket polarity, perhaps implying an effect of the hydroxy group of BHT on the Fe−CO fragment (*10*). It is noted that the ν(Fe−CO) band appears somewhat sharper in the spectra of the butylated hydroxytoluene-bound samples, perhaps indicating the FeCO fragments are somewhat more flexible in the substrate-free and benzphetamine-bound cases. It is noted that although there is an apparent effect on the ν(Fe−CO) mode, all of the low-frequency *heme* modes are unaffected; the ν_8 mode is found at 348 cm^{-1}, while peripheral group bending modes are assigned to bands at 376 cm^{-1} (propionate bending) and an envelope of bands centered around 415 cm^{-1} (vinyl bending).

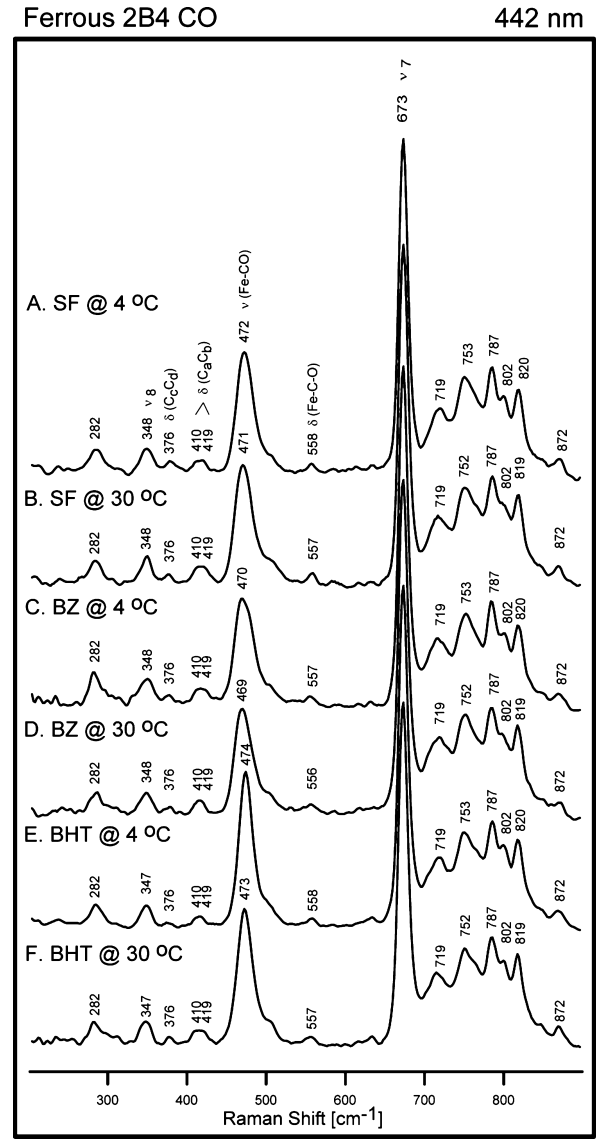

FIGURE 8: Low-frequency resonance Raman spectra of ferrous CO adducts of P450 2B4 without (spectra A and B) and with substrates [spectra C and D with benzphetamine (BZ); spectra E and F with butylated hydroxytoluene (BHT)] at 4 and 30 °C. Excitation line 442 nm, 1 mW on the sample, total collection time 10 min (spectra normalized to the ν_7 mode at 673 cm^{-1}).

The high-frequency RR spectra of ferrous CO adducts of substrate-free and both substrate-bound samples at 4 and 30 °C are displayed in Figure S3. There it is shown that all of the high-frequency marker modes for all samples studied show no significant shifts upon substrate variation (Figure S3). This behavior is in agreement with all previous studies of P450 CO adducts (*15, 34, 35*) and is also consistent with the lack of the substrate effect on the *low-frequency* heme modes mentioned above (Figure 8). However, the relatively intense feature appearing at 1556 cm^{-1} in Figure S3, most reasonably assigned to ν_{11} (*55*), warrants special attention inasmuch as it shows rather substantial sensitivity to interactions with redox partners, as described below.

(2) Effects of Redox Partner: Mn(III) Cyt b_5 and P450 Reductase on Ferrous CO P450 2B4. Figures S4 and S5 show the RR spectra of the ferrous CO adducts of substrate-

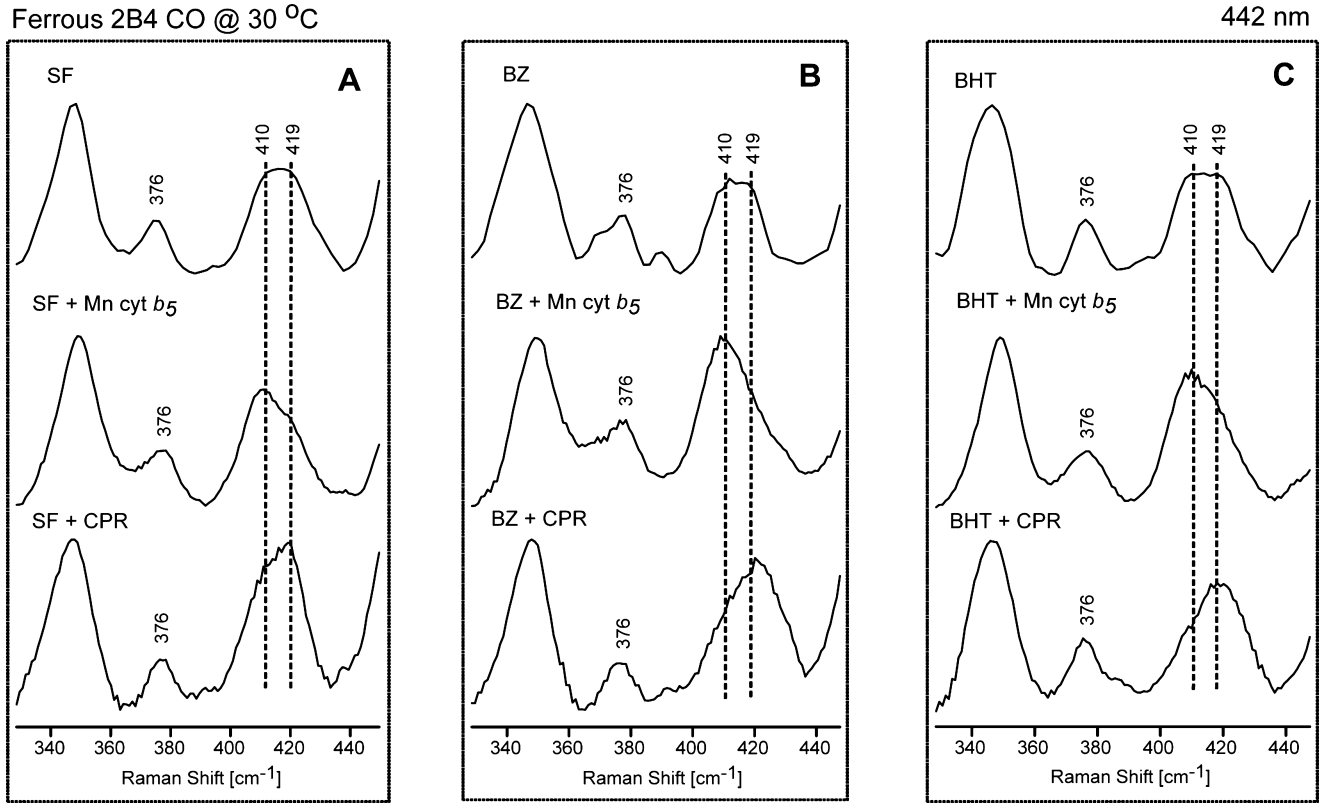

FIGURE 9: Comparison of the expanded low-frequency region of substrate-free (panel A), benzphetamine-bound (panel B), and butylated hydroxytoluene-bound (panel C) ferrous CO cytochrome P450 2B4 in the absence of redox partner (upper traces) and in the presence of Mn(III) cytochrome b_5 (middle traces) and P450 reductase (bottom traces). Traces are taken from Figures 8, S4, and S5.

free and both substrate-bound forms of P450 2B4 in the presence of Mn cyt b_5 and CPR, respectively. There it is seen that, for all of the samples studied, the addition of either redox partner does not affect the position of the ν(Fe−CO) mode. Interestingly, the only region that is clearly affected is that associated with vinyl bending modes that occur between 400 and 440 cm^{-1}. This envelope of bands is more clearly defined in Figure 9, which shows the 330–450 cm^{-1} region for all ferrous CO samples studied (at 30 °C). Two roughly equal intensity vinyl bending modes appear at 410 and 419 cm^{-1} for all samples that lack a redox partner (top three traces). In the complex with Mn cyt b_5 the 410 cm^{-1} feature is enhanced, while the 419 cm^{-1} feature decreases in intensity. Interestingly, the effect of interaction with CPR is again opposite to that observed with the cyt b_5, showing selective enhancement of the *higher* frequency component at the expense of the lower one (bottom three traces in Figure 9). There are vinyl groups at positions 2 and 4 of the macrocycle, and it is noted that the assignments of the vinyl bending modes to the 2- and 4-vinyl groups for any given protein are firmly established only by difficult and time-consuming vinyl labeling, which is not yet available for this or any other P450. However, the normally accepted framework, mainly based on work for labeled myoglobins (*48, 56*), is to assign a higher frequency bending mode to out-of-plane (oop) and a lower frequency one to planar (*18*). Here that framework is followed with no attempt being made to specify the relative planar/perpendicular populations of the individual (2- vs 4-) vinyl groups. Finally, although it is noted that structural data are available for crystals of several different forms of cytochrome P450 2B4, including a dimeric form of substrate-free (*44*) and two different inhibitor-bound forms (*57, 58*), comparison of these, using Mercury 1.4.2 software, reveals that the 2-vinyl groups display quite small differences in disposition and that while the 4-vinyl group of the substrate-free form is displaced to the opposite side of the heme compared to the other two, the torsional angle is within about 10° of that for either of the inhibitor-bound forms. Since there are no striking differences in angles among the groups, and especially because it is not clear which, if any, of these structures would correspond to a given reductase-bound form being studied here, no clear insight is provided by trying to relate these structural parameters to our spectroscopic data.

On the basis of the above considerations, the RR spectral data obtained here provide definitive evidence that CPR causes active site perturbations that generate more out-of-plane vinyl groups, while the cyt b_5 interaction leads to a higher fraction of *in-plane* vinyl groups. Despite these apparent changes in the vinyl bending modes, there are no obvious changes in the ν(C═C) vinyl *stretching* modes seen at 1620 cm^{-1} in Figures S3, S6, and S7. However, this is not problematical since detailed analyses of the dependence of high-frequency vinyl stretching modes for systems with known vinyl group orientations (measured with a torsional angle designated as τ) have shown that similar ν(C═C) frequencies can be obtained for vinyl groups having quite different orientations; e.g., a vinyl group that is nearly planar ($\tau = 2.3°$) and one that is almost perpendicular ($\tau = -97.8°$) both have ν(C═C) frequencies at 1621 cm^{-1} (*59*). Importantly, as discussed in part C, these vinyl bending mode changes are potentially useful in deducing perturbations in the electronic structure of the heme macrocycle that may hold implications for reactivity.

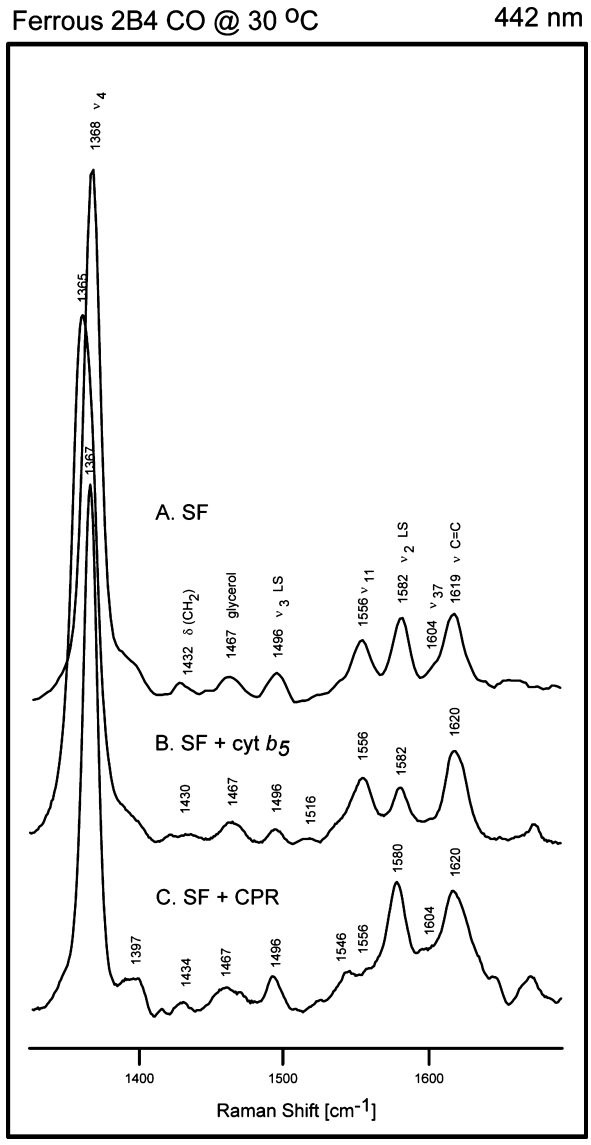

FIGURE 10: Comparison of the expanded high-frequency region of susbtrate-free ferrous CO cytochrome P450 2B4 in the absence of redox partner (A) and in the presence of Mn(III) cytochrome b_5 (B) and P450 reductase (C). Traces are taken from Figures S3, S6, and S7, respectively.

With the exception of the changes seen for the combined effect of BZ and cyt b_5 binding to $Fe^{2+}CO$ P450 mentioned above, it is noted that no such low-frequency spectral changes were induced upon binding of redox partners to *ferric* P450 2B4; this difference may be attributable to the fact that the vinyl substituents are believed to occupy a more highly conjugated, in-plane orientation with respect to the mean heme in the reduced forms of P450s (*18*) and thereby become more sensitive to protein-induced alterations. This suggestion also would be consistent with the aforementioned behavior of the ν_{11} mode at 1556 cm^{-1}, all data being shown in Figures S3, S6, and S7, with those for the SF form being collected in Figure 10 for easy reference to the following discussion. Thus, binding of Mn cyt b_5 enhances the lower frequency vinyl bending mode (panel A of Figure 9) and gives rise to an apparent intensity enhancement of the ν_{11} mode (Figure 10), while binding of CPR enhances the *higher* frequency vinyl mode (Figure 9, panel A) and essentially abolishes the ν_{11} intensity (Figure 10). This behavior reflects a connection between the vinyl group disposition and the intensity of the ν_{11} mode, the latter containing substantial contributions from the $C_\beta-C_\beta$ stretching coordinate of heme pyrrole rings, which can couple with the ν(C=C) vinyl stretch (see ref *48* for heme atom labeling). While it might be expected that ν_2, which is also associated with the $C_\beta-C_\beta$ coordinate, would also be so affected, no strong correlation is observed. The most likely explanation for this contrasting behavior is the fact that while ν_2 is a totally symmetric mode expected to be enhanced under Soret excitation, the nontotally symmetric ν_{11} mode gains such intensity in response to symmetry lowering associated with vinyl group conjugation, with a higher population of planar form being expected to give increased ν_{11} intensity (*8, 9, 48*). Finally, the one other obvious effect of the redox partner is the observed 3 cm^{-1} downshift in ν_4 that occurs only upon interaction with the Mn cyt b_5. This shift to lower frequency is most reasonably attributed to the increase in vinyl group planarity, which can act to reduce electron density in the filled macrocycle π-bonding orbitals (*18, 60, 61*).

In trying to relate these data to any previous work, it is necessary to point out that there are very few RR data available regarding the interaction of ferrous CO adducts of other P450s with their redox partners (Table 1). The addition of putitaredoxin to the ferrous CO adduct of camphor-bound P450cam causes only a 2 cm^{-1} upshift of the ν(Fe−CO) mode (*62*). Similarly, the addition of adrenodoxin to mitochondrial P450scc shifts the ν(Fe−CO) only by 0–2 cm^{-1} depending upon the structure of the added substrate (*31*). Thus, the relative insensitivity of the ν(Fe−CO) to binding of redox partners observed here is consistent with these two previous reports. However, the rather definitive changes observed here for the vinyl bending and ν_{11} modes reflect a reorientation of the vinyl groups, apparently in different directions, upon binding of CPR or cyt b_5, alterations that may potentially impact function (*vide infra*).

(C) Biochemical Implications. In the absence of substrate, the P450 2B4 samples employed here contain small amounts of high-spin component and undergo minimal conversion from the low-spin to high-spin state at higher temperatures. However, interaction with BZ or BHT substrates causes a significant low-spin to high-spin conversion, even at 4 °C, with the extent of this conversion substantially increasing at 30 °C, presumably because of enhanced substrate binding which displaces the sixth axial ligand, water. The detailed RR studies undertaken here do reveal that while substrate binding induces a low- to high-spin conversion by displacing a water ligand from the heme iron, neither the heme structure nor the cysteine−thiolate linkage of the ferric heme resting state is especially sensitive to substrate structure. Even in the case of the ligated ferrous CO form, substrate structure has a small impact on the Fe−CO fragment. Thus, addition of benzphetamine causes a 2 cm^{-1} *downshift* of ν(Fe−CO) mode, whereas butylated hydroxytoluene causes a 2 cm^{-1} *upshift* of this mode, with the BHT-bound adduct apparently experiencing a slightly more polar and less flexible environment, i.e., a slightly higher frequency and a narrower bandwidth. Nevertheless, these are indeed relatively small effects compared to those seen for the bacterial P450s where substrate binding has been shown to cause shifts of nearly 20 cm^{-1} (*15, 16*). Thus, the presence of substrate, and

Table 1: Frequencies (cm^{-1}) of the Fe−CO Fragment Modes and ν(Fe−S) Modes of Known P450s

protein	redox partner	ν(Fe−CO)	δ(Fe−C−O)	ν(Fe−S)	ref
P450cam					
substrate-free		464	556		*15*
+camphor		481	558		*15*
+camphor		482.5	561.4	351	*62*
+camphor	putidaredoxin	484.9	561.5		*62*
+camphor	cyt b_5	483	561	351	*62*
+camphor				350.5	*51*
+camphor	putidaredoxin			353.3	*51*
+adamantanone				350.5	*51*
+norcamphor				349.7	*51*
+TMCH[a]				349.4	*51*
P450cam					
+camphor		484	562		*19*
P450cam D251N					
+camphor		484	561		*19*
P450cam T252A					
+camphor		483	562		*19*
$P450_{BS\beta}$					
substrate-free		488	587		*34*
+myristic acid		491	587		*34*
BM3 heme domain					
substrate-free		471	558		*35*
+palmitate		471	557		*35*
+arachidonic acid				356	*18*
$P450_{scc}$					
substrate-free		476			*31*
substrate-free	adrenodoxin	476			*31*
+cholesterol		482			*31*
+cholesterol	adrenodoxin	483.5			*31*
+25-OH-cholesterol		484			*31*
+25-OH-cholesterol	adrenodoxin	484			*31*
+22(*R*)-OH-cholesterol		479			*31*
+22(*R*)-OH-cholesterol	adrenodoxin	480			*31*
+22(*S*)-OH-cholesterol		487			*31*
+22(*S*)-OH-cholesterol	adrenodoxin	488			*31*
P450arom					
substrate-free		477	555		*28*
+androstenedione (AD)		485	557	349	*28*
+testosterone		484	555	349	*28*
+19-OH-AD				346	*28*
+19-aldo-AD		490	561	344	*28*
+19-nor-AD		501	563	349	*28*
P450 2B4		4 °C/30 °C	4 °C/30 °C	30 °C	
substrate-free		472/471	558/557		this work
+BZ		470/469	557/556	354	this work
+BHT		474/473	558/557	354	this work
substrate-free	Mn cyt b_5	472/471	559/559		this work
+BZ	Mn cyt b_5	470/469	558/558	352	this work
+BHT	Mn cyt b_5	474/473	560/559	352	this work
substrate-free	CPR	472/471	558/557		this work
+BZ	CPR	470/469	559/558	354	this work
+BHT	CPR	474/473	558/557	354	this work
P450 2D6					
substrate-free		477 (476)			*30* (*29*)
+DX[b]		482 (481)			*30* (*29*)
+BF[c]		477			*30*
+MDMA[d]		482			*30*
P450 2D6 T309V					
substrate-free		476			*29*
+DX[b]		481			*29*
P450 2D6 F120A					
substrate-free		477			*30*
+DX[b]		477			*30*
+BF[c]		477			*30*
+MDMA[d]		477			*30*

[a] 3,3,5,5-Tetramethylcyclohexanone. [b] Dextromethorphan hydrobromide. [c] Bufuralol hydrochloride. [d] 3,4-Methylenedioxymethylamphetamine.

differences in substrate structure, has relatively small impact on the disposition of bound ligands.

On the other hand, the interactions with the two redox partners studied here, which both bind on the proximal surface of P450 2B4 near the axial cysteine (*37, 52*), differentially affect the active site structures of both the ferric and CO-ligated ferrous derivatives. Specifically, upon interaction with the resting state and substrate-bound CYP 2B4, Mn cyt b_5 increases the high-spin form while CPR causes an apparent, though slight, decrease of the high-spin form of the ferric P450. Consistent with this, Mn cyt b_5 decreases the Fe−S bond strength in the ferric high-spin state, whereas

CPR does not significantly alter this key linkage. Interestingly, the combined effects of BZ and cyt b_5 binding cause unique changes in the low-frequency region, with two additional vinyl bending modes being observed near 403 and 430 cm^{-1}; the behavior of these modes, as explained later, is often associated with predictable changes in the heme reduction potential. Finally, while the increased population of the more readily reducible high-spin state of the ferric enzyme induced by interaction of cyt b_5, but not CPR, would be expected to possibly enhance catalytic turnover by facilitating electron transfer (*32*), there are no relevant biological consequences of this effect, inasmuch as it is known that, because of its high potential, cyt b_5 is incompetent to deliver the first electron to produce the ferrous P450 2B4 (*5, 47*).

While the identity of the associated reductase apparently has no effect on the distal side of the heme pocket, as judged by the lack of any changes in the ν(Fe−CO) mode, it is shown that CPR and cyt b_5 differentially affect the P450 2B4 active site structure in ways that alter the dispositions of the peripheral vinyl groups of the heme, as documented by intensity differences in the vinyl bending modes appearing between 410 and 420 cm^{-1}. Thus, while Mn cyt b_5 selectively enhanced the 410 cm^{-1} (in-plane) vinyl bending mode and increased the intensity of ν_{11}, the presence of CPR had opposite effects, deactivating the ν_{11} mode and selectively enhancing the 419 cm^{-1} vinyl bending mode; as noted above, the intensity of the nontotally symmetric ν_{11} mode is expected to increase as vinyl group planarity (conjugation) increases.

These changes in vinyl group planarity may have biochemical consequences inasmuch as it was shown previously that the orientation of vinyl substituents, as well as propionate groups, and their interaction with protein environment affect the heme redox potential (*18, 60, 61*). Specifically, for metalloporphyrins the electron-withdrawing properties depend on the degree of coplanarity of vinyl groups and the heme macrocycle; a larger in-plane population of vinyls stabilizes the ferrous state and leads to a higher reduction potential. The lower frequency vinyl bending mode, associated with the in-plane conformation, is more populated in the presence of Mn cyt b_5 compared to P450 2B4 without any redox partner, implying a higher heme reduction potential (*18*). Significantly, the binding of CPR has an opposite effect on P450 2B4, yielding a higher population of the out-of-plane vinyl group, based on the increased intensity of the ~420 cm^{-1} feature, and implying a decrease in reduction potential. While these considerations lead to the expectation that the ferrous ligated P450 2B4 could be more readily reduced in the presence of cyt b_5 than for the corresponding complex with CPR, the effect must be small, inasmuch as it has been shown that both cyt b_5 and P450 reductase reduce the ferrous dioxygen adduct at similar rates (*5, 47*).

Perhaps the most likely cause of the demonstrated ability of cyt b_5 to increase catalytic turnover for CYP 2B4 is the proposed enhanced proton transfer to the fleeting hydroperoxo intermediate for the complex with cyt b_5 compared to that with CPR (*5, 47*). While this proposal is not directly addressed by the series of current studies, planned future work involving radiolytic reduction, and subsequent annealing, of cryotrapped dioxygen complexes may be capable of detecting differences in proton delivery efficiencies (*20, 63*).

SUPPORTING INFORMATION AVAILABLE

Seven figures showing low-frequency RR spectra of ferric and ferrous P450 2B4 in the presence of cyt b_5 and CPR and high-frequency RR spectra of P450 2B4 ferrous CO adducts in the presence of redox partners. This material is available free of charge via the Internet at http://pubs.acs.org.

REFERENCES

1. Coon, M. J. (2005) Cytochrome P450: Nature's Most Versatile Biological Catalyst. *Annu. Rev. Pharmacol. Toxicol. 45*, 1–25.
2. Guengerich, P. F. (2007) Mechanisms of cytochrome P450 substrate oxidation. *J. Biochem. Toxicol. 21*, 163–168.
3. Ortiz de Montellano, P. R. (2005) *Cytochrome P450: Structure, Mechanism, and Biochemistry* (Ortiz de Montellano, P. R., Ed.) Kluwer Academics/Plenum, New York.
4. Zhao, Y., and Halpert, J. R. (2007) Structure-function analysis of cytochromes P450 2B. *Biochim. Biophys. Acta 1770*, 402–412.
5. Zhang, H., Im, S.-C., and Waskell, L. (2007) Cyt b_5 increases the rate of product formation by cytochrome P450 2B4 and competes with cytochrome P450 reductase for a binding site on cytochrome P450 2B4. *J. Biol. Chem. 282*, 29766–29776.
6. Shengxi, J., Bryson, T. A., and Dawson, J. H. (2004) Hydroperoxoferric heme intermediate as a second electrophilic oxidant in cytochrome P450-catalyzed reactions. *J. Biol. Inorg. Chem. 9*, 644–653.
7. Chandrasena, R., Esala, P., Vatsis, K. P., Coon, M. J., Hollenberg, P. F., and Newcomb, M. (2004) Hydroxylation by the Hydroperoxy-Iron Species in Cytochrome P450 Enzymes. *J. Am. Chem. Soc. 126*, 115–126.
8. Spiro, T. G. (1988) *Biological Applications of Raman Spectroscopy* (Spiro, T. G. , Ed.) Vol. III, John Wiley and Sons, New York.
9. Kincaid, J. R. (2000) Resonance Raman spectra of heme proteins and model compounds, in *Porphyrin Handbook* (Kadish, K. M., Smith, K. M., and Guilard, R., Eds.) Vol. 7, pp 225–291, Academic Press, New York.
10. Ray, G. B., Li, X. Y., Ibers, J. A., Sessler, J. L., and Spiro, T. G. (1994) How far can proteins bend the FeCO unit? Distal polar and steric effects in heme proteins and models. *J. Am. Chem. Soc. 116*, 162–176.
11. Rousseau, D. G., and Rousseau, D. L. (1992) Hydrogen bonding of iron-coordinated histidine in heme proteins. *J. Struct. Biol. 109*, 13–17.
12. Ozaki, Y., Kitagawa, T., Kyogoku, Y., Shimada, H., Iizuka, T., and Ishimura, Y. (1976) An anomaly in the resonance Raman spectra of cytochrome P-450cam in the ferrous high-spin state. *J. Biochem. (Tokyo) 80*, 1447–1451.
13. Champion, P. M., Gunsalus, I. C., and Wagner, G. C. (1978) Resonance Raman investigations of cytochrome P450cam from *Pseudomonas putida*. *J. Am. Chem. Soc. 100*, 3743–3751.
14. Champion, P. M., Stallard, B. R., Wagner, G. C., and Gunsalus, I. C. (1982) Resonance Raman detection of an iron-sulfur bond in cytochrome P 450cam. *J. Am. Chem. Soc. 104*, 5469–5472.
15. Uno, T., Nishimura, Y., Makino, R., Iizuka, T., Ishimura, Y., and Tsuboi, M. (1985) The resonance Raman frequencies of the iron-carbon monoxide stretching and bending modes in the carbon monoxide complex of cytochrome P-450cam. *J. Biol. Chem. 260*, 2023–2026.
16. Wells, A. V., Li, P., Champion, P. M., Martinis, S. A., and Sligar, S. G. (1992) Resonance Raman investigations of *Escherichia coli*-expressed *Pseudomonas putida* cytochrome P450 and P420. *Biochemistry 31*, 4384–4393.
17. Macdonald, I. D. G., Sligar, S. G., Christian, J. F., Unno, M., and Champion, P. M. (1999) Identification of the Fe-O-O Bending Mode in Oxycytochrome P450cam by Resonance Raman Spectroscopy. *J. Am. Chem. Soc. 121*, 376–380.
18. Chen, Z., Ost, T. W. B., and Schelvis, J. P. M. (2004) Phe393 Mutants of Cytochrome P450 BM3 with Modified Heme Redox Potentials Have Altered Heme Vinyl and Propionate Conformations. *Biochemistry 43*, 1798–1808.
19. Deng, T.-J., Macdonald, I. D. G., Simianu, M. C., Sykora, M., Kincaid, J. R., and Sligar, S. G. (2001) Hydrogen-Bonding Interactions in the Active Sites of Cytochrome P450cam and Its Site-Directed Mutants. *J. Am. Chem. Soc. 123*, 269–278.
20. Mak, P. J., Denisov, I. G., Victoria, D., Makris, T. M., Deng, T.-J., Sligar, S. G., and Kincaid, J. R. (2007) Resonance Raman

Detection of the Hydroperoxo Intermediate in the Cytochrome P450 Enzymatic Cycle. *J. Am. Chem. Soc. 129*, 6382–6383.
21. Hildebrandt, P., Greinert, R., Stier, A., Stockburger, M., and Taniguchi, H. (1988) Surface enhanced resonance Raman study of phenobarbital-induced rabbit liver cytochrome P-450 LM2. *FEBS Lett. 227*, 76–80.
22. Hildebrandt, P., Garda, H., Stier, A., Stockburger, M., and Van Dyke, R. A. (1988) Resonance Raman study of the cytochrome P-450 LM2-halothane intermediate complex. *FEBS Lett. 237*, 15–20.
23. Hildebrandt, P., Greinert, R., Stier, A., and Taniguchi, H. (1989) Resonance Raman study on the structure of the active sites of microsomal cytochrome P-450 isozymes LM2 and LM4. *Eur. J. Biochem./FEBS 186*, 291–302.
24. Hildebrandt, P., Garda, H., Stier, A., Bachmanova, G. I., Kanaeva, I. P., and Archakov, A. I. (1989) Protein-protein interactions in microsomal cytochrome P-450 isozyme LM2 and their effect on substrate binding. *Eur. J. Biochem./FEBS 186*, 383–388.
25. Hildebrandt, P., Heibel, G., Anzenbacher, P., Lange, R., Kruger, V., and Stier, A. (1994) Conformational analysis of mitochondrial and microsomal cytochrome P-450 by resonance Raman spectroscopy. *Biochemistry 33*, 12920–12929.
26. Macdonald, I. D. G., Smith, G. C. M., Graeme, C. M., Wolf, C. R., and Smith, W. E. (1996) Observation of structural variation and spin state conversion of cytochrome P450 CYP2B4 on binding of sterically different substrates. *Biochem. Biophys. Res. Commun. 226*, 51–58.
27. Tomita, T., Ogo, S., Egawa, T., Shimada, H., Okamoto, N., Imai, Y., Watanabe, Y., Ishimura, Y., and Kitagawa, T. (2001) Elucidation of the differences between the 430- and 455-nm absorbing forms of P450-isocyanide adducts by resonance Raman spectroscopy. *J. Biol. Chem. 276*, 36261–36267.
28. Tosha, T., Kagawa, N., Ohta, T., Yoshioka, S., Waterman, M. R., and Kitagawa, T. (2006) Raman Evidence for Specific Substrate-Induced Structural Changes in the Heme Pocket of Human Cytochrome P450 Aromatase during the Three Consecutive Oxygen Activation Steps. *Biochemistry 45*, 5631–5640.
29. Bonifacio, A., Groenhof, A. R., Keizers, P. H. J., Graaf, Ch., Commandeur, J. N. M., Vermeulen, N. P. E., Ehlers, A. W., Lammertsma, K., Gooijer, C., and Van der Zwan, G. (2007) Altered spin state equilibrium in the T309V mutant of cytochrome P450 2D6: a spectroscopic and computational study. *J. Biol. Inorg. Chem. 12*, 645–654.
30. Bonifacio, A., Keizers, P. H. J., Commandeur, J. N. M., Vermeulen, N. P. E., Robert, B., Gooijer, C., and Van der Zwan, G. (2006) Binding of bufuralol, dextromethorphan, and 3,4-methylenedioxymethylamphetamine to wild-type and F120A mutant cytochrome P450 2D6 studied by resonance Raman spectroscopy. *Biochem. Biophys. Res. Commun. 343*, 772–779.
31. Tsubaki, M., Yoshikawa, S., Ichikawa, Y., and Yu, N.-T. (1992) Effects of cholesterol side-chain groups and adrenodoxin binding on the vibrational modes of carbon monoxide bound to cytochrome P-450scc: implications of the productive and nonproductive substrate bindings. *Biochemistry 31*, 8991–8999.
32. Sligar, S. G. (1976) Coupling of spin, substrate, and redox equilibria in cytochrome P450. *Biochemistry 15*, 5399–5406.
33. Gruenke, L. D., Sun, J., Loehr, T. M., and Waskell, L. (1997) Resonance Raman spectral properties and stability of manganese protoporphyrin IX cytochrome b_5. *Biochemistry 36*, 7114–7125.
34. Matsunaga, I., Yamada, A., Lee, D.-S., Obayashi, E., Fujiwara, N., Kobayashi, K., Ogura, H., and Shiro, Y. (2002) Enzymatic reaction of hydrogen peroxide-dependent peroxygenase cytochrome P450s: kinetic deuterium isotope effects and analyses by resonance Raman spectroscopy. *Biochemistry 41*, 1886–1892.
35. Deng, T.-J., Proniewicz, L. M., Kincaid, J. R., Yeom, H., Macdonald, I. D. G., and Sligar, S. G. (1999) Resonance Raman Studies of Cytochrome P450BM3 and Its Complexes with Exogenous Ligands. *Biochemistry 38*, 13699–13706.
36. Miroux, B., and Walker, J. E. (1996) Over-production of proteins in *Escherichia coli*: mutant hosts that allow synthesis of some membrane proteins and globular proteins at high levels. *J. Mol. Biol. 260*, 289–298.
37. Bridges, A., Gruenke, L., Chang, Y. T., Vakser, I. A., Loew, G., and Waskell, L. (1998) Identification of the binding site on cytochrome P450 2B4 for cytochrome b_5 and cytochrome P450 reductase. *J. Biol. Chem. 273*, 17036–17049.
38. Shen, A. L., Porter, T. D., Wilson, T. E., and Kasper, C. B. (1989) Structural analysis of the FMN binding domain of NADPH-cytochrome P-450 oxidoreductase by site-directed mutagenesis. *J. Biol. Chem. 264*, 7584–7589.
39. Mulrooney, S. B., and Waskell, L. (2000) High-level expression in *Escherichia coli* and purification of the membrane-bound form of cytochrome b_5. *Protein Expression Purif. 19*, 173–178.
40. Morgan, E. T., and Coon, M. J. (1984) Effects of cytochrome b_5 on cytochrome P-450-catalyzed reactions. Studies with manganese-substituted cytochrome b_5. *Drug Metab. Dispos. 12*, 358–364.
41. Omura, T., and Sato, R. (1964) The carbon monoxide-binding pigment of liver microsomes. II. Solubilization, purification, and properties. *J. Biol. Chem. 239*, 2379–2385.
42. Vermilion, J. L., and Coon, M. J. (1978) Purified liver microsomal NADPH-cytochrome P-450 reductase. Spectral characterization of oxidation-reduction states. *J. Biol. Chem. 253*, 2694–2704.
43. Estabrook, R. W., and Werringloer, J. (1978) The measurement of difference spectra: application to the cytochromes of microsomes. *Methods Enzymol. 52*, 212–220.
44. Scott, E. E., He, Y. A., Wester, M. R., White, M. A., Chin, C. C., Halpert, J. R., Johnson, E. F., and Stout, C. D. (2003) An open conformation of mammalian cytochrome P 450 2B4 at 1.6-Å resolution. *Proc. Natl. Acad. Sci. U.S.A. 100*, 13196–13201.
45. Li, X.-Y., Czernuszewicz, R. S., Kincaid, J. R., and Spiro, T. G. (1989) Consistent porphyrin force field. 3. Out-of-plane modes in the resonance Raman spectra of planar and ruffled nickel octaethylporphyrin. *J. Am. Chem. Soc. 111*, 7012–7023.
46. Li, X.-Y., Czernuszewicz, R. S., Kincaid, J. R., Stein, P., and Spiro, T. G. (1990) Consistent porphyrin force field. 2. Nickel octaethylporphyrin skeletal and substituent mode assignments from nitrogen-15, meso-d4, and methylene-d16 Raman and infrared isotope shifts. *J. Phys. Chem. 94*, 47–61.
47. Zhang, H., Gruenke, L., Arscott, D., Harris, D. L., Glavanovich, M., Johnson, R., and Waskell, L. A. (2003) Determination of the Rate of Reduction of Oxyferrous Cytochrome P450 2B4 by 5-Deazariboflavin Adenine Dinucleotide T491V Cytochrome P450 Reductase. *Biochemistry 42*, 11594–11603.
48. Hu, S., Smith, K. M., and Spiro, T. G. (1996) Assignment of protoheme resonance Raman spectrum by heme labeling in myoglobin. *J. Am. Chem. Soc. 118*, 12638–12646.
49. Mak, P. J., Podstawka, E., Kincaid, J. R., and Proniewicz, L. M. (2004) Effects of Systematic Peripheral Group Deuteration on the Low-Frequency Resonance Raman Spectra of Myoglobin Derivatives. *Biopolymers 75*, 217–228.
50. Hu, S., Morris, I. K., Singh, J. P., Smith, K. M., and Spiro, T. G. (1993) Complete assignment of cytochrome c resonance Raman spectra via enzymic reconstitution with isotopically labeled hemes. *J. Am. Chem. Soc. 115*, 12446–12458.
51. Unno, M., Christian, J. F., Benson, D. E., Gerber, N. C., Sligar, S. G., and Champion, P. M. (1997) Resonance Raman investigations of cytochrome P450cam complexed with putidaredoxin. *J. Am. Chem. Soc. 119*, 6614–6620.
52. Zhang, H., Myshkin, E., and Waskell, L. (2005) Role of cytochrome b_5 in catalysis by cytochrome P450 2B4. *Biochem. Biophys. Res. Commun. 338*, 499–506.
53. French, J. S., Guengerich, F. P., and Coon, M. J. (1980) Interactions of cytochrome P-450, NADPH-cytochrome P-450 reductase, phospholipid, and substrate in the reconstituted liver microsomal enzyme system. *J. Biol. Chem. 255*, 4112–4119.
54. Hasemann, C. A., Kurumbail, R. G., Boddupalli, S. S., Peterson, J. A., and Deisenhofer, J. (1995) Structure and function of cytochromes P450: a comparative analysis of three crystal structures. *Structure 3*, 41–62.
55. Wang, J., Stuehr, D. J., and Rousseau, D. L. (1997) Interactions between substrate analogues and heme ligands in nitric oxide synthase. *Biochemistry 36*, 4595–4606.
56. Smulevich, G., Hu, S., Rodgers, K. R., Goodin, D. B., Smith, K. M., and Spiro, T. G. (1996) Heme-protein interactions in cytochrome *c* peroxidase revealed by site-directed mutagenesis and resonance Raman spectra of isotopically labeled hemes. *Biospectroscopy 2*, 365–376.
57. Scott, E. E., White, M. A., He, Y. A., Johnson, E. F., Stout, C. D., and Halpert, J. R. (2004) Structure of Mammalian Cytochrome P450 2B4 Complexed with 4-(4-Chlorophenyl)imidazole at 1.9-Å Resolution: Insight into the Range of P450 Conformations and the Coordination of Redox. *J. Biol. Chem. 279*, 27294–27301.
58. Zhao, Y., White, M. A., Muralidhara, B. K., Sun, L., Halpert, J. R., and Stout, C. D. (2006) Structure of Microsomal Cytochrome P450 2B4 Complexed with the Antifungal Drug Bifonazole: insight into P450 conformational plasticity and membrane interaction. *J. Biol. Chem. 281*, 5973–5981.

59. Marzocchi, M. P., and Smulevich, G. (2003) Relationship between heme vinyl conformation and the protein matrix in peroxidases. *J. Raman Spectrosc. 34*, 725–736.

60. Reid, L. S., Lim, A. R., and Mauk, A. G. (1986) Role of heme vinyl groups in cytochrome b_5 electron transfer. *J. Am. Chem. Soc. 108*, 8197–8201.

61. Lee, K.-B., Jun, E., La Mar, G. N., Rezzano, I. N., Pandey, R. K., Smith, K. M., Walker, F. A., and Buttlaire, D. H. (1991) Influence of heme vinyl- and carboxylate-protein contacts on structure and redox properties of bovine cytochrome b_5. *J. Am. Chem. Soc. 113*, 3576–3583.

62. Unno, M., Christian, J. F., Sjodin, T., Benson, D. E., Macdonald, I. D. G., Sligar, S. G., and Champion, P. M. (2002) Complex formation of cytochrome P450cam with putidaredoxin. Ecidence for protein-specific interactions involving the proximal thiolate ligand. *J. Biol. Chem. 277*, 2547–2553.

63. Davydov, R., Makris, T. M., Kofman, V., Werst, D. E., Sligar, S. G., and Hoffman, B. M. (2001) Hydroxylation of Camphor by Reduced Oxy-Cytochrome P450cam: Mechanistic Implications of EPR and ENDOR Studies of Catalytic Intermediates in Native and Mutant Enzymes. *J. Am. Chem. Soc. 123*, 1403–1415.

BI800034B